DRAFT VERSION APRIL 23, 2019
Typeset using LaTeX **modern** style in AASTeX62

HD106906 Working Papers

YIFAN ZHOU[1]

[1]*Steward Observatory*

ABSTRACT

This documents keep the main result for *Cloud Atlas* HD106906b (Bailey et al. 2013) observations.

Todo list

1. INTRODUCTION

HD106906b is a mid-L type planetary mass companion (Bailey et al. 2013).

2. OBSERVATIONS

The observations of HD106906 are part of HST large treasure program *Cloud Atlas* (Program ID: 14241, PI: D. Apai). We used HST/WFC3/IR to observe HD106906 from 2016-01-29 20:45 to 2016-01-29 23:02 UTC for two consecutive HST orbits as part of the program variability amplitude assessment survey (VAAS). We then used the same instrument to observe the target from 2018-06-07 02:14 to 2018-06-07 12:35 for seven consecutive HST orbits for deep look observations (DLO). Light curves in F127M ($\lambda_{\rm pivot} = 1.274\mu$m, FWHM = 0.07), F139M ($\lambda_{\rm pivot} = 1.384\mu$m, FWHM = 0.07) and F153M $\lambda_{\rm pivot} = 1.533\mu$m, FWHM = 0.07 filters were taken in both observations. Exposure times were 66.4 seconds for the F127M and F153M frames and 88.4 seconds for the F139M frames. Filters rotated for every two to three frames through the entire observation sequences. Consequently, the observations in three filters were effectively simultaneous. The filter selection facilitated our goal of comparing HD106906b's rotational modulation in (F139M) and out of (F127M, F153M) the 1.4 μmwater absorption band.

Primary star subtraction is required for precision photometry of HD106906b because of the moderate contrast between the companion and its host star. The observation was set to enable two-roll differential imaging that could effectively subtract the point spread function (PSF) of the primary star. Between every two adjacent HST orbits, the position angle of

Corresponding author: Yifan Zhou
yzhou@as.arizona.edu

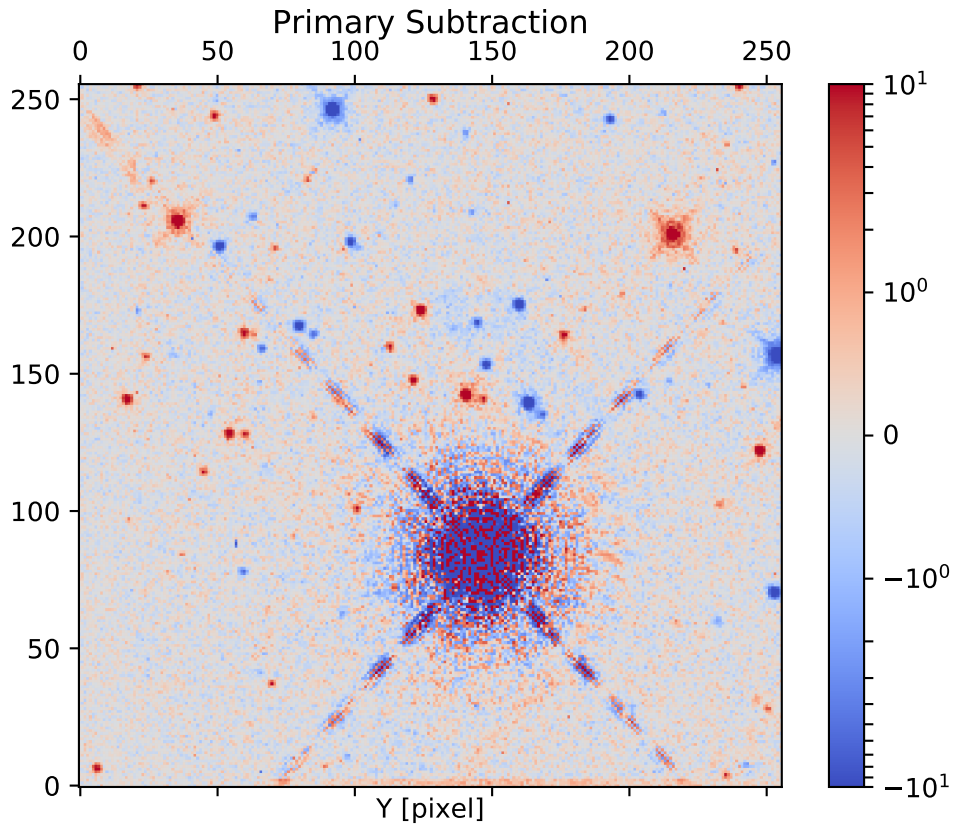

Figure 1. Two-roll differential imaging result.

the telescope differed by 31 degrees. In this way the position angle of the companion to the host star in the image reference frame had the same difference between images from two orbits (Figure). Image subtraction removed the PSF structures that were associated with the telescope optical assembly but conserved the astrophysical signal, which primarily was HD106906b's PSF.

add figure

In total, we obtained 19 frames for each filter in the VAAS observation and 63 frames for each filter in the DLO observation. The photometric signal-to-noise ratio (SNR) for HD106906b was $\sim$ 100 per frame.

3. DATA REDUCTIONS

Time-resolved photometry for HD106906b started with `flt` frames produced by CALWFC3. This data reduction component included four steps: image preparation, primary star subtraction, PSF fitting photometry, and light curve systematics removal.

Image preparation sorted `flt` frames into data cubes for subsequent image processing. Before place images into data cubes, we first made bad pixel mask and remove sky background for every frame. Pixels that have data quality flags 4 (bad detector pixel), 16 (hot pixel), 32(unstable response), and 256 (full-well saturation) were identified as "bad pixels" and excluded from subsequent analyses. After masking out pixels with those data quality flags, we examined the imaged by eye to identify and mask remaining spurious pixels. To

remove sky background, we first drew circular masks around all visible point sources in the field and then applied a five-iteration sigma-clip to further exclude bright pixels. The median value of the unmasked pixel was the sky background and removed from the images. The background removed images as well as the associated bad pixel masks were sorted by time and formed the data cube.

We then applies two-roll differential imaging (2RDI) to subtract the PSF of HD106906AB. First, we registered the images by the centroid of HD106906AB. The centroid coordinates of HD106906AB were measured relative to those of the first image frame using two-dimensional cross-correlation and further refined by residual least χ^2 minimization in the diffraction spider region. We then selected best PSF image from candidate PSF image. Every image that was taken with different telescope roll angles as the target image was a candidate PSF. The candidate PSF was linearly scaled to minimize the least squared residual in an annulus around HD106906AB (Figure 1), and the best PSF was the one that has the smallest residuals. Finally, we subtract the best PSFs from original images and obtained primary subtracted images (Figure 1).

Show the optimization region

HD106906b's photometry was measured by PSF fitting to the primary subtracted images. We construct 9× over-sampled PSFs using TINYTIM. Free parameters for the model PSFs were the centroid coordinates, HST secondary mirror displacement, and the scale of the PSF. We optimized these parameters by χ^2 minimization, which was performed by Markov Chain Monte Carlos. We normalized the total flux for the model PSF with an infinite large radius. Therefore the best fit scale of the PSF was the total flux of HD106906b with that includes aperture correction. We use the World Coordinate System information that are in the fits file header to convert the centroid coordinates to RA and DEC astrometry.

The uncertainties of light curves in F127M, F139M, and F153M are all dominated by random noise that includes photon noise, readout noise, and dark current. However, light curve analyses require systematic noise in the light curve to be accurately characterized and corrected. For WFC3/IR light curves, charge trapping related ramp effect is the major component of the systematic noise. We use RECTE (Zhou et al. 2017) to model and remove the ramp effect systematics from the light curves. The ramp effect removal procedure follows Zhou et al. (2019) that details the application of RECTE in time-resolved direct imaging observations. We calculate ramp profiles by feeding the entire direct image time series into RECTE and forward-modeling the charge trapping processes. The model ramp profiles are then divided from the uncorrected light curves, which results in corrected light curves.

4. RESULTS

4.1. *Photometry, light curves and variability*

We obtained single frame photometry at SNRs of 77, 78, and 105 in the F127M, F139M, and F153M bands, respectively. After aperture correction, the absolute flux intensity in these three bands are $6.23 \pm 0.08 \times 10^{-13}$ergs cm^{-2} s^{-1} μm^{-1}, $3.71 \pm 0.05 \times 10^{-13}$ergs cm^{-2} s^{-1} μm^{-1}, and $4.35 \pm 0.04 \times 10^{-13}$ergs cm^{-2} s^{-1} μm^{-1}, respectively. The flux uncertainty are for average $1-\sigma$ uncertainty in a single frame. Figure 2 shows the

corrected and normalized light curve in the F127M, F139M, and F153M bands. No large amplitude ($> 1\%$) rotational modulations are identifiable in all three light curves. Variations in the light curve are dominated by random noise whose major component is photon noise. Comparing to flat lines, the three light curves have reduced-χ^2 of 1.89, 1.47, and 1.1 for the F127M, F139M, and F153M bands, respectively.

To investigate light curve periodicity, we derived the power spectra for the light curves using Lomb-Scargle periodogram method (Lomb 1976, Figure 3). The power spectra for the F139M and F153M light curves do not have any significant peaks except in the high frequency ends of the power spectra, which are dominated by random noise. The lack of structures in the F139M and F153M power spectra is consistent with the featureless light curves. The power spectra for the F127M light curve does clearly peaks at 4.02 hr. Fitting a single 4.02 hr sine wave to the F127M light curve marginally decreases the reduced-χ^2 from 1.89 (for a flat line) to 1.53. The best-fitting parameters of the 4.02 hr sine wave are amplitude $= 0.49 \pm 0.12\%$, phase $= -1.57 \pm 0.29$ rad. Figure 4 shows the F127M light curve folded to the 4.02 hr period.

In summary, HD106906b shows marginal evidence of variability in the F127M band, which is the bluest band in the observations. Light curves in the other two bands (water absorption, red side of water band continuum) are consistent with flat lines.

4.2. *Spectral Energy Distribution*

We combine our photometry results with archival data to investigate the spectral energy distribution (SED) of HD106906b. We take HST/ACS/F606W band ($\lambda_{\rm pivot} = 0.596\mu$m, FWHM$= 0.234\mu$m) from Kalas et al. (2015), K_s ($\lambda_{\rm pivot} = 2.145\mu$m, FWHM$= 0.305\mu$m) and L' ($\lambda_{\rm pivot} = 3.774\mu$m, FWHM$= 0.592\mu$m) bands from Bailey et al. (2013). We do not use the archival J band photometry because our F127M photometry characterizes similar spectral features and has more than 20$\times$ greater SNR. Our F139M photometry provide a tight 1.4μm water absorption constraint for HD106906b.

We fit the SED of HD106906b to the BT Settl (Allard et al. 2012, Figure 5). We perform model fitting in magnitude scale, for which we convert the flux intensity to magnitude and linearly interpolate the model grid in magnitude scales. The free parameters are effective temperature $T_{\rm eff}$, surface gravity $\log g$, and a scaling parameter. Because the model SED is presented as the flux at the photosphere surface, with known distance the scaling parameter can be translate to the photospheric radius. Using least χ^2 criterion, we result in best-fitting $T_{\rm eff}$ of $1,800 \pm 100$ K and $\log g = 5.5 \pm 0.5$. The scaling parameter corresponds to a radius of $1.775 pm 0.015 R_{\rm Jup}$ at a distance of 103.3 pc (Gaia Collaboration et al. 2018, 2016). The 1,800 K effective temperature estimate is consistent with previous study (Bailey et al. 2013; Wu et al. 2016), but the surface gravity is not compatible with a low surface gravity assessment. In addition, the model SED under-predicts the F139M band flux, or over-predicts the depth of the water absorption band.

4.3. *Astrometry*

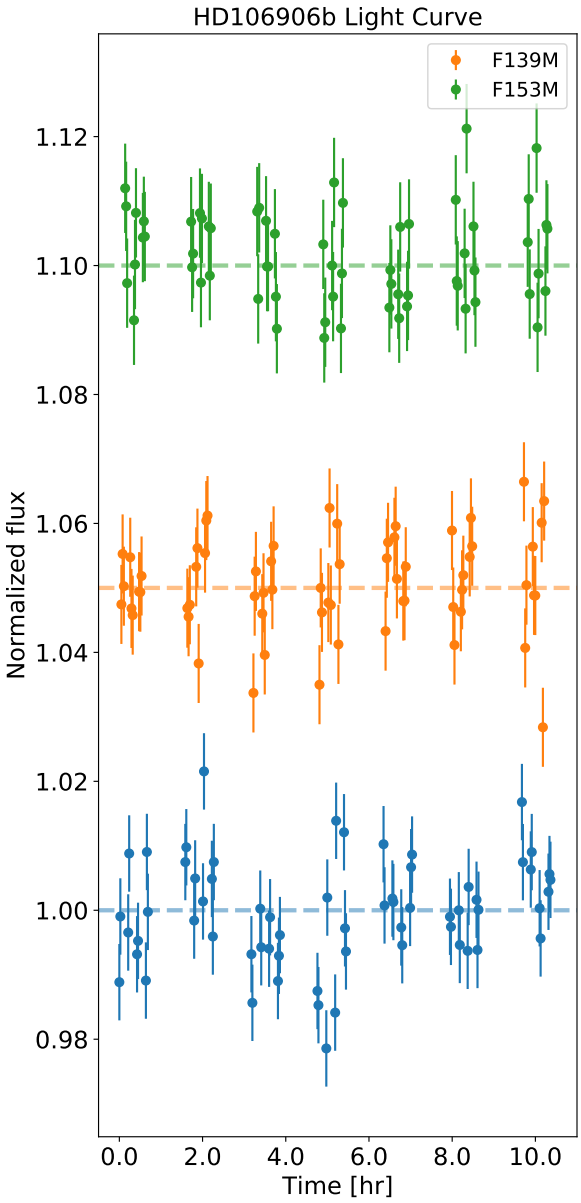

Figure 2. The light curve for HD106906b in the F127M, F139M, and F153M

We are particularly interested in the background star that is only 0″.87 away from HD106906b, because it is unreported in previous studies and could contaminate the photometric and spectroscopic observations of HD106906b. We calculated the differences in right ascension (ΔRA) and declination (ΔDEC) and the separations between HD106906b and the background star from year 2003 (one year before the first direct imaging record of HD106906b) to year 2023. In this calculation, the background star is assumed to be stationary and HD106906b is co-moving with its host star at ($\mu_\alpha \cos\delta = -39.01$mas/yr, $\mu_\delta = -12.87$mas/yr) (Gaia Collaboration et al. 2016, 2018). The results are shown in Figure 6. In the same figures, we also marked the previous observations (Bailey et al. 2013; Wu et al. 2016; Lagrange et al. 2016; Daemgen et al. 2017) to evaluate if the background star was detectable or could contaminate the measurements in those observations.

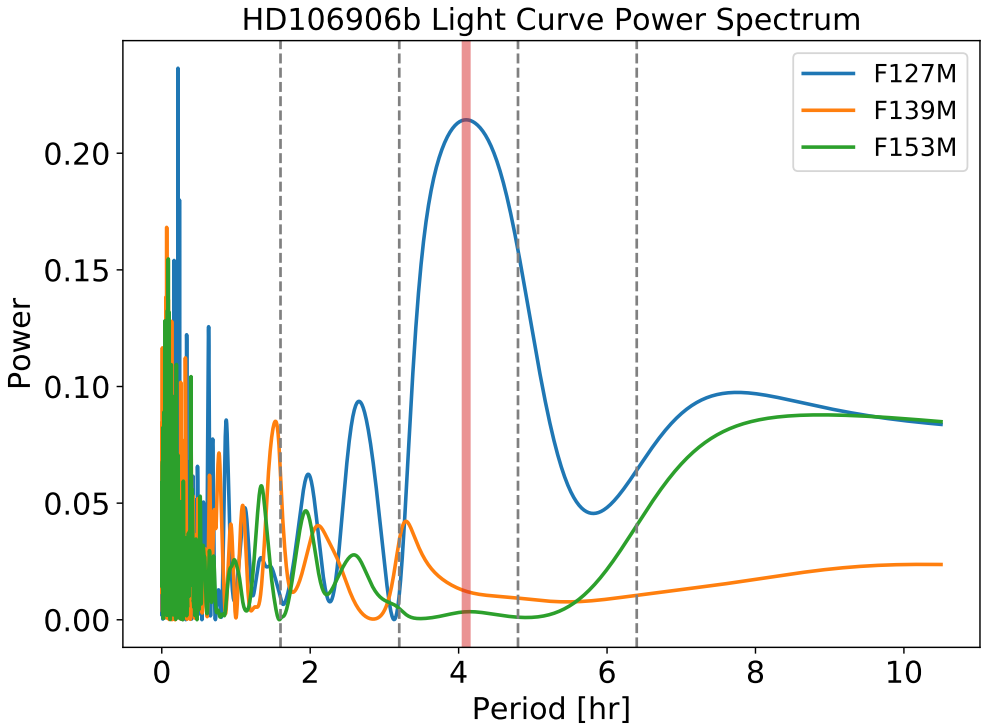

Figure 3. Lomb-Scargle periodogram for the light curves of HD106906b.

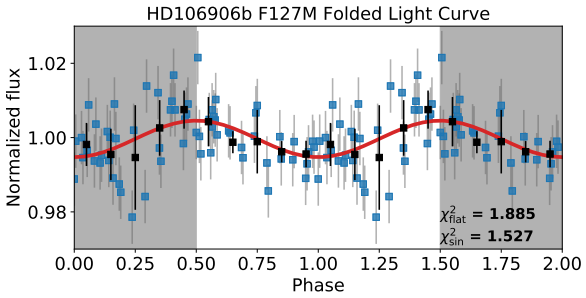

Figure 4. Phase-folded light curve for F127M. The light curve is folded to a period of 4.02 hr. The period corresponds to the most significant peak in the Lomb Scargle periodogram.

Figure 6 demonstrates that HD106906b, due to its proper motion, has been approaching the background star over the years. The separation between these two object has shortened from 1″.29 (2004, first imaging record) to 0″.87 (this study). In the study of (Bailey et al. 2013; Wu et al. 2016; Daemgen et al. 2017), the background star had separation of 0.95-1.05 to HD106906b. Given their separations in these studies, it is unclear if the background star contaminated those measurements. Considering the brightness contrast of the two object, in the worst case, the contamination of the background star to HD106906b's broadband photometry is $< 7.5\%$.

4.4. *Other sources in the field*

Our 30″×30″ field of view (Figure 7) is a crowded field that may include yet undiscovered companion of HD106906. The three filters that are used in this observation measure the

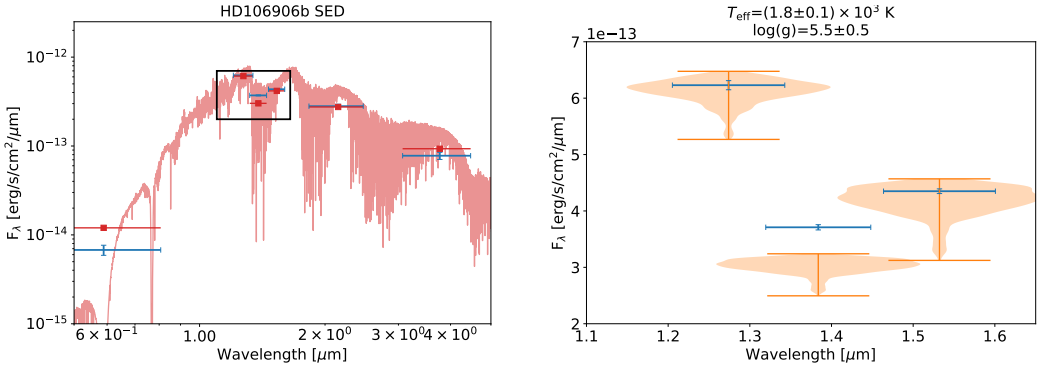

Figure 5. The SED of HD106906 and the best-fitting BT Settl model. The left panel shows the full observed SED (blue) that includes photometry from both this observation and archival data. The red line is the best-fitting BT Settl spectrum (1800 K, $\log g = 5.5$). The red dots are the model photometry that are from model spectrum integrated with the filter throughput curves. The right panel zooms in the wavelength range of this observation. The orange violin plot shows the uncertainty of the model fitting. The flux in the F139M band is significantly under-predicted by the BT Settl model.

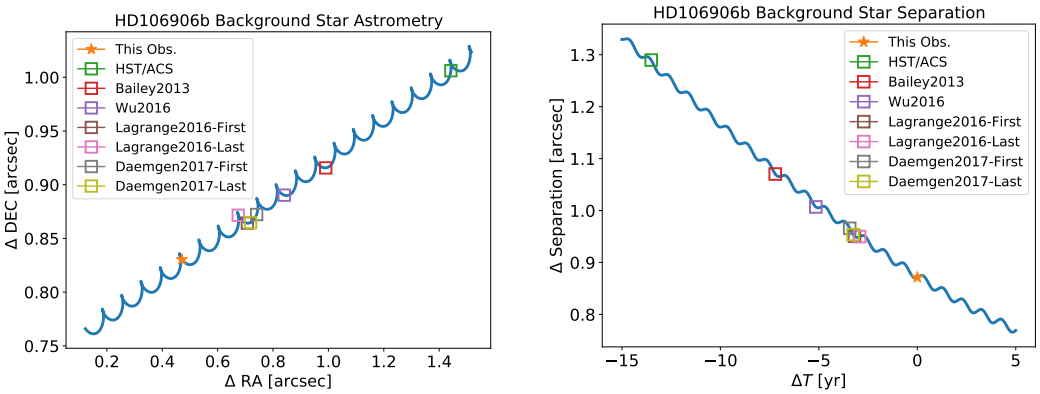

Figure 6. Relative astrometry between HD106906b and a closeby background star. Left: The difference in right ascension and declination. Right: The separation as a function of time. Past observations of HD106906b are marked as squares.

water absorption depth, which is an effective criterion to select ultra-cool objects. Here we define the water absorption depth as the difference between the F139M flux intensity and the continuum, which is average flux intensity of F127M and F153M. This difference is further normalized by the continuum flux to get the relative water absorption depth. The relative water absorption depth is calculated as the following equation.

$$D = \frac{(f_{\rm F127M} + f_{\rm F153M})/2 - f_{\rm F139M}}{(f_{\rm F127M} + f_{\rm F153M})/2} \quad (1)$$

We used the median combined primary subtracted image to measure the relative water absorption depth for 12 point sources (include HD106906b) that are in the field of view for both telescope rolls. Figure 8 shows the water absorption depth for each source. Except HD106906b, there is one source that has significant water absorption depth. Interestingly, this source is the one that is discussed in §4.3, and also the one that has the smallest angular separation to HD106906b among all sources in the field of view. However, based on the

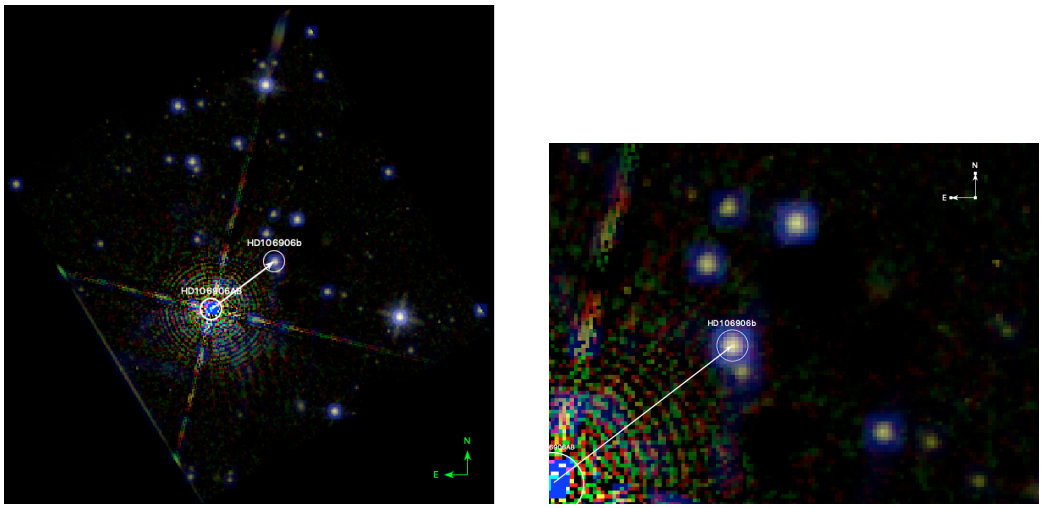

Figure 7. R (F153M) G (F139M) B (F127M) images of HD106906 (left) and the zoomed-in view of the planet. The PSF of the planet has less green shade compared to background stars due to strong water absorption of HD106906b.

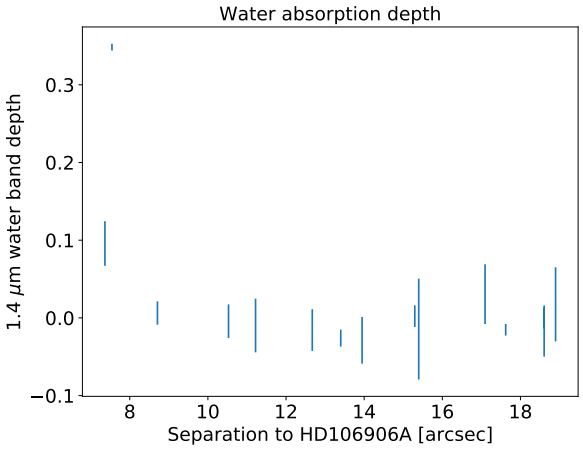

Figure 8. Water absorption depths of all sources in the field of view. The sources are ranked by their angular distance to HD106906AB. The two sources (one is HD106906b) that have significant water absorption are also the two that are closest to HD106906AB in agnular distance.

discussion of §4.3, this source is unlikely to be co-moving with HD106906. Its astrometry is consistent of being a background star.

5. DISCUSSION

1. variability:]
   color dependence, compare with other planetary mass companions
2. the limit on the inclination (see Vos et al. 2018)
3. SED of HD106906. Deviation from BT Settl model. The best-fitting $\log g$ is very high (5.5)
4. possible astrometry constrains (what about the distortion correction for WFC3)

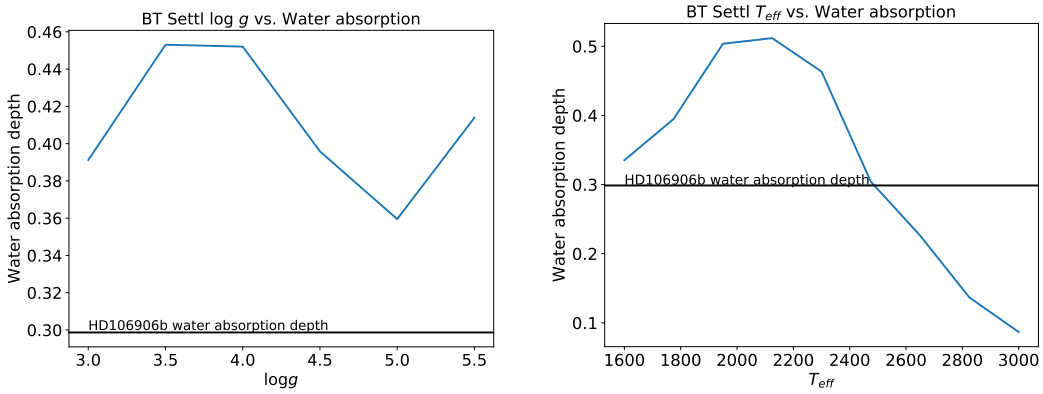

Figure 9. 1.4 μm water band depths predicted by the BT Settl model. Left: With a fixed $T_{\rm eff} = 1800$ K, models with log g between 3 to 5.5 all over-predicts the water band depths. Right: With a fixed log $g = 5.5$, it requires $T_{\rm eff} = 2500$ K for the model to match the observation.

5. limit on additional companions

5.1. *SED of HD106906b*

Two issues have emerged in the SED fitting results. First, the best-fitting model over-predicts the 1.4 μm water absorption band depth. Second, the best-fitting surface gravity is inconsistent with previous low-gravity assessment for HD106906b.

To investigate the first issue, we calculate the water band absorption depths in the BT Settl as functions of $T_{\rm eff}$ and log g and compare them with the observed value. As shown in Figure 9), for a fixed $T_{\rm eff}$ of 1800 K, all BT Settl models over-predict the water band depth. For a fixed log g of 5.5, to match the observed water band depth, $T_{\rm eff}$ needs to be raised to 2500 K, although such a high temperature is not at all consistent with the overall SED shape. Therefore, the mismatch between the HD106906b's observed and the model SEDs in the 1.4 μm water bands demonstrates the inadequacy of current state-of-the-art ultra-cool atmospheric models.

Bailey et al. (2013) and Daemgen et al. (2017) have discussed the surface gravity of HD106906b. Both studies classify HD106906b as a low-to-intermediate surface gravity object based on its triangle-shaped H band spectrum. The equivalent widths of the K I absorption lines measured in Daemgen et al. (2017) are also consistent with an intermediate surface gravity classification. In addition, low surface gravity is also consistent with the young and low mass nature of HD106906b. However, our SED fitting yield a very high gravity result. With a fixed $T_{\rm eff}$ of 1800 K, lower surface gravity models significantly over-predicts the F153M and $K_{\rm s}$ band flux intensities, therefore they are not preferred by the SED fitting. This inconsistency, again, may show the insufficiency of atmospheric models for planetary-mass ultra-cool objects.

REFERENCES

Allard, F., Homeier, D., & Freytag, B. 2012, Philos. Trans. A. Math. Phys. Eng. Sci., 370, 2765

Bailey, V., Meshkat, T., Reiter, M., et al. 2013, ApJ, 780, L4

Daemgen, S., Todorov, K., Quanz, S. P., et al. 2017, A&A, 608, A71
Gaia Collaboration, Brown, A. G. A., Vallenari, A., et al. 2018, A&A, 616, A1
Gaia Collaboration, Brown, A. G. A., Vallenari, A., Prusti, T., et al. 2016, A&A, 595, A2
Kalas, P. G., Rajan, A., Wang, J. J., et al. 2015, ApJ, 814, 32
Lagrange, A.-M., Langlois, M., Gratton, R., et al. 2016, A&A, 586, L8
Lomb, N. R. 1976, Astrophys. Space Sci., 39, 447
Vos, J. M., Allers, K. N., Biller, B. A., et al. 2018, MNRAS, 474, 1041
Wu, Y.-L., Close, L. M., Bailey, V. P., et al. 2016, ApJ, 823
Zhou, Y., Apai, D., Lew, B. W. P., & Schneider, G. H. 2017, AJ, 153, 243
Zhou, Y., Apai, D., Lew, B. W. P., et al. 2019, AJ, 157, 128